SECTION 4 - THEORETICAL COMPARISON OF REACTORS

This section is divided into five areas:

4.1 The Fischer-Tropsch Mechanism
4.2 The Reactor Models
4.3 Discussion of Results
4.4 Conclusions
4.5 Mechanism Improvements

A reasonable mathematical description of Fischer-Tropsch kinetics is essential to a successful modeling effort. Section 4.1 describes the approach taken in the development of the mechanism, the requirements and assumptions built into the mathematics, and the resultant product rate expressions.

Section 4.2 discusses the incorporation of the mechanism into the three different reactor models. The heat and weight balance equations used for each system, as well as the necessary support subroutines, are discussed in detail. A description of the capabilities built into each reactor model concludes Section 4.2.

Section 4.3 is divided as follows:

1. Data Fitting
2. Reactor Variable Studies, and
3. Reactor Comparisons

Data fitting is a very important part of any modeling effort in that it gives a direct indication of the reliability of the model. In this case, reasonable agreement of fit parameters common to all three reactor systems suggests that the equations chosen to describe the mechanism and reactor systems are good approximations. Section 4.3 describes the approach used in the selection of fit parameters and the results of the data fitting.

Confidence generated in the system equations through data fitting naturally leads to the exploration of operating parameter effects on conversion and product yield structure. These variable studies are presented for each reactor system.

The final objective of the modeling effort is to compare the Fischer-Tropsch reactor systems for inherent strengths and/or weaknesses. The end of Section 4.3 discusses these reactor comparisons and coupled with the physical comparison of reactors (Section 5) provides a foundation for the overall conclusions presented in the Summary.

Section 4.4 lists conclusions based only on the theoretical comparisons.

Although the mechanism discussed in Section 4.1 is capable of describing gross product yields and, therefore, fulfills the requirements of this report, a more in-depth understanding of Fischer-Tropsch reactor systems can be gained by the incorporation of certain mechanism improvements. Section 4.5 discusses these improvements and describes their incorporation into the original mechanism.

4.1 MECHANISM

Anderson, et al. (30), Vannice (31), Catalytica Associates, Inc. (32), Oak Ridge (33), and Ponec (34), have all given excellent reviews of the existing theories on mechanisms for the Fischer-Tropsch reaction. In general, the vast majority of the data are discussed in terms of three mechanisms: the hydroxy-carbene mechanism, the formyl mechanism, and the carbide mechanism. At various points in Fischer-Tropsch history, each of these has been generally favored over the other two, and none of them can be clearly eliminated from consideration. Even though each has its own distinctive active intermediate, there is still a great deal of commonality among the mechanisms.

This commonality is the foundation for the four <u>minimum</u> criteria that must be met to adequately describe the Fischer-Tropsch mechanism:

A. The mechanism must be a polymerization process. For the Fischer-Tropsch reaction, this involves the formation of an active species followed by propagation of alkyl chains, one carbon at a time until termination occurs by severing the catalyst-carbon bond. This, then, leaves an active species available to begin the chain propagation again.

B. The mechanism must be consistent with the generation of normal paraffins and olefins as primary products. This is consistent with the polymerization process described above, and typifies the product yields obtained from iron catalysts. The remainder of the product consists primarily of oxygenates, aromatics, and branched olefins and paraffins (30-34).

C. The mechanism must reflect the non-selective nature of the carbon number distribution as described by the Schulz-Flory analysis (35). With the exception of the light hydrocarbons, i.e., C_1-C_5, a plot of the natural log of the mole fraction of carbon numbered species versus the carbon numbers closely approximates a straight line. By making the assumption that all hydrocarbon species on the catalyst surface have an equal probability to add a carbon and form an oligomer one carbon longer, Schulz and Flory (35) were able to statistically predict the Fischer-Tropsch product distribution by carbon number. The above assumption led to an equation of the form:

$$X_n = p^{n-1}(1-p) \tag{1}$$

which when put in log form becomes:

$$\ln X_n = n \ln p + \ln \frac{1-p}{p} \tag{2}$$

This can be seen to be the equation of a straight line with slope, ln p, and intercept, $\frac{1-p}{p}$. Knowing p, one can now calculate a term called the "Degree of Polymerization" which is defined as:

$$DP = \frac{1}{1-p} \tag{3}$$

The degree of polymerization is a measure of the extent of the polymerization reaction. It can also be used to describe the average Fischer-Tropsch product distribution. For example, Figure 4.1-1 represents the weight fraction of C_n versus n at different degrees of polymerization (32). It should be noted that as DP increases, the product distribution becomes very broad. At a DP equal to 6, the C_6 oligomer is the most abundant species on a weight basis, but only accounts for 7 wt-% of the total product. This truly is a characteristic of the Fischer-Tropsch reaction and is an indication of the non-selective nature of the polymerization process.

D. The mechanism should incorporate an equilibrium between the olefins on the catalyst sites and the olefins in the surrounding gas or liquid (36, 37). The paraffin production is a termination reaction, and the evidence that paraffins do not initiate new chains or insert into existing chains is strong (37, 38, 39). For olefins and oxygenates, the evidence is that they are reactive and, although it is not completely clear, appear to be reactive largely through chain initiation (38-41). In explaining the mechanism of the bi-functional Fischer-Tropsch catalyst, P. D. Caesar, et al. (36), proposed that "Chain propagation by coordination of α-olefins becomes the major route in iron Fischer-Tropsch chemistry as the reaction temperature is raised from 250-350°C". It seems likely, then, that there is an equilibrium, either chemical or physical, between the olefins on the catalyst sites and the olefins in the gas or liquid surrounding the catalyst particles.

Figure 4.1-2 is a schematic representation of the mechanism used in all the reactor models. M represents an "active" metal site. Whether M is a carbide, hydroxy-carbene, or a formyl structure is not important. It is merely a location where chain propagation can occur. The polymerization process proceeds by addition of CO and hydrogen to an alkyl chain, $M(CH_2)_{n-1}H$, forming another alkyl chain one carbon longer, $M(CH_2)_nH$, while liberating H_2O. This process is continued from $M(CH_2)_nH$ to $M(CH_2)_{n+1}H$, and so forth.

Two reactions are responsible for the production of the primary products. The first is the hydrogenation of an alkyl chain of any length to form a paraffin. The second is an equilibrium adsorption-desorption step to form an olefin. In both cases, when the active intermediate is "terminated", another initiation site, MH, is created, which can again participate in chain growth by reacting with CO and H_2. The mechanism, therefore, operates with a constant number of active catalyst sites. This is important if the mechanism is expected to reflect a Schulz-Flory distribution of products.

In the development of this mechanism and in the development of the rate expressions which describe the mechanism, some important assumptions were made. These were as follows:

A. Since oxygenated products, excluding H_2O and CO_2, seem to be formed in a manner similar to olefins and since the quantity formed is small for most Fischer-Tropsch catalysts, oxygenates are not considered at this time.

B. Branched olefins and paraffins are considered to be produced from the recoordination of olefins, i.e., the reattachment of olefins to the metal site. Recoordination is part of the proposed mechanism. However, distinction between recoordination of olefins in the branched form versus the unbranched form is not made.

C. Aromatics are considered to be small enough fractions of the total product to be eliminated from consideration at this time.

D. Catalyst deactivation is not considered.

E. The formation of free carbon is not considered, neither is the second route to methane through free carbon suggested by Dry (6).

F. The Schulz-Flory assumption that "All hydrocarbon species on the catalyst surface have an equal probability to add a carbon and form an oligomer one carbon longer," in kinetic terms suggests that the rate

constant for polymerization is a constant function for all carbon numbers. This assumption is adopted not only for the polymerization rate constants but also for the paraffin termination and olefin formation rate constants.

G. The powers on all reactant and product concentration terms in the mechanism are assumed to be unity.

H. The steady state assumption is used on the rates of formation of all metal site complexes.

I. The total number of "active" metal sites is assumed to be constant, i.e.,

$$[CAT] = MH + M(CH_2)H + \sum_{j=2}^{n} M(CH_2)_jH = \text{CONSTANT} \qquad (4)$$

Performance data in the literature show clear limitations to some of these assumptions. However, they are adequate for a first test of the mechanism on real data and for evaluation of gross product changes as a function of reactor design and operating conditions.

Based on these assumptions, then, the final product rate expressions (as derived in Appendix A) are:

Methane

$$r_{CH_4} = C\, k_H\, [H_2]\; [MH] \qquad (5)$$

Paraffins $n \geq 2$

$$r_{C_nH_{2n+2}} = \left(A^{n-1}\, C + B \sum_{i=2}^{n} A^{n-i}[C_iH_{2i}]\right) k_H[H_2]\; [MH] \qquad (6)$$

Olefins $n \geq 2$

$$r_{C_nH_{2n}} = \left[k_o \left(A^{n-1} C + B \sum_{i=2}^{n} A^{n-i} [C_iH_{2i}]\right) - \frac{k_o}{K_e} [C_nH_{2n}]\right] [MH] \quad (7)$$

The simplified rate expression adopted for the water-gas shift is as follows:

$$r_{WG} = k_{WG} \left([CO][H_2O] - \frac{1}{K_{e_{WG}}} [CO_2][H_2]\right) [CAT] \quad (8)$$

It is assumed that this reaction proceeds in parallel with the Fischer-Tropsch reaction. Since Fischer-Tropsch catalysts have shift activity, the rate of reaction is assumed to be proportional to the catalyst concentration [CAT]. However, as it is not known whether the shift reaction requires the same active metal site as the Fischer-Tropsch reaction, it was decided that it should not compete for the same catalyst sites. Therefore, in this study the shift reaction is not assumed to be proportional to available Fischer-Tropsch initiation sites [MH], neither does it influence their concentration. The importance of the shift reaction to the understanding of the differences between reactor systems is discussed later in this report.

FIGURE 4.1-1

HYDROCARBON DISTRIBUTION FROM SCHULZ-FLORY POLYMERIZATION

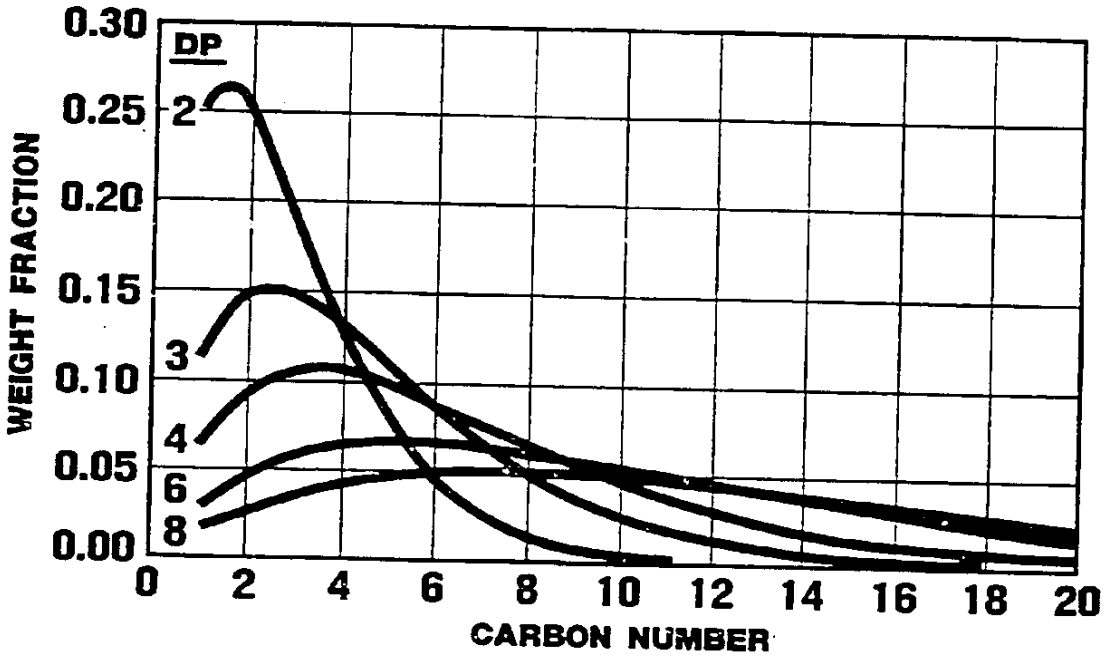

UOP 573-66

FIGURE 4.1-2
MECHANISM

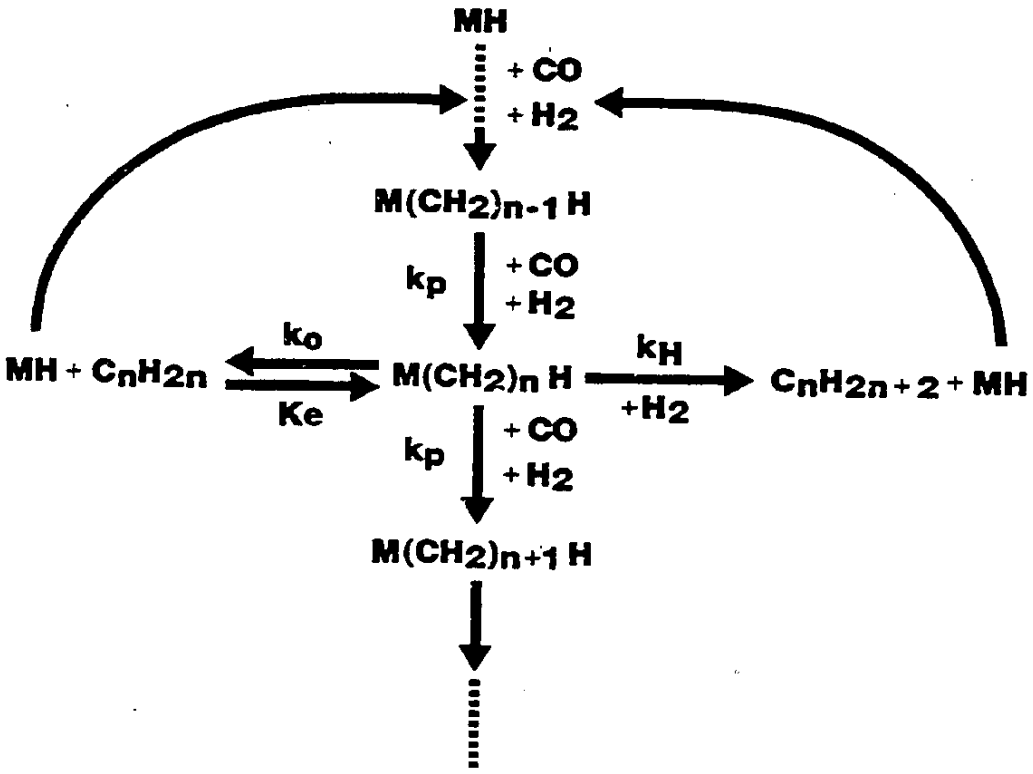

4.2 REACTOR MODELING

4.2.1 Modular Approach

It was critical in the development of the mathematical model to distinguish between system differences caused by reactor characteristics and differences caused by computer logic error. It was toward this end that a modular approach to programming was considered.

In the modular system any calculation procedures that are common to all reactor systems are put into a common subroutine which can then be incorporated into each reactor system. The obvious advantage is that the calculations are identical for all systems. In actual practice, however, a complete module is rarely identical for all reactor systems. A modified modular approach was therefore used in which "identical calculations" were supplemented for each reactor system. These modules now perform the same function in each reactor model and have identical core calculation procedures, but are tailored for the individual reactor systems.

A "modular" diagram which represents the basic logic flow of the three reactor models is illustrated in Figure 4.2-1. A few of the modules are unique to a given model as indicated. The basic flow consists of the usual input and output sections with the core of each program being the REACTOR module. This module contains the basic mass and energy balances for each system, and draws on a variety of support modules to provide the necessary information to complete its function. A description of each of the modules follows.

4.2.1.1 Input, Output of Input, and Setup

The INPUT module provides all of the information necessary for the computer models to function. A list of the input parameters for each program is provided in the Appendix B.

The module labeled OUTPUT OF INPUT prints out the input and is merely a convenience, so the programmer can check for errors in the input parameters.

The SETUP module manipulates the input parameters for eventual use in the REACTOR module. For example, if a volumetric flow rate is required in the REACTOR module, but a molar flow rate is used as an input parameter, the SETUP module will convert molar flow to volumetric flow assuming an ideal gas.

4.2.1.2 Physical Properties Linkage, Dew Point and Liquid Properties

These modules are unique to the slurry reactor model. They are used as a link to UOP "in-house" programs which are capable of supplying all component physical properties as well as performing basic thermodynamic operations on any process stream.

4.2.1.3 Hydraulics

Pressure drop in the tube-wall reactor and in the slurry reactor is negligible when compared to the operating pressure. For these models it is, therefore, assumed that the reactor operates at a uniform pressure and hydraulic calculations are not required. However, this is not the case for the entrained bed reactor. Kellogg in its Synthol Feasibility Study (4) reported pressure drops of as much as 80 psi. Not only is this pressure drop significant, but its magnitude can be appreciably altered by operating conditions such as catalyst loading, i.e., pounds of catalyst per cubic foot of gas fed to the reactor. A UOP "in-house" calculation procedure is used as a basis for the HYDRAULICS module incorporated into the entrained bed reactor model, and calculates a pressure profile and catalyst loading through the reactor based on the operating conditions chosen.

4.2.1.4 Heat Balance Information

The function of this module is to supply heat of reaction and heat capacity information to the REACTOR module. The heats of reactions are calculated on a per mole of CO converted basis using heats of formations at 300°C obtained from "Selected Values of Physical and Thermodynamic Properties of Hydrocarbons and Related Compounds" issued by the American

Petroleum Institute Research Project-44. The values and equations used for these calculations can be found in Appendix C.

The heat capacities of the various components were obtained from Smith and Van Ness (42). The values and equations used for these calculations can also be found in Appendix C.

4.2.1.5 Heat Transfer Information

In the tube-wall and entrained bed reactors, heat of reaction is removed by heat exchange within the reactor system. It is, therefore, necessary to calculate an overall heat transfer coefficient.

The tubular reactor model has the capability of operating as two different reactor systems, i.e., a fixed bed tubular reactor and a flame-sprayed tube-wall reactor. The resistances to heat transfer due to the metal wall and due to the coolant film obviously exist in both cases, but the resistance due to the film on the reactant side does not exist in the case of the tube-wall reactor. In this case, the reaction takes place on the flame-sprayed catalyst which is physically part of the tube wall. Because of the potential instability of cocurrent and countercurrent cooling systems described by Degnan and Wei (43), a boiling cooling media (Dowtherm) was selected. The high heat transfer coefficient and constant coolant temperature, combined with the large amount of cooling surface inherent to the tube-wall reactor, results in very little temperature variation along this reactor. The calculation procedure has, therefore, been simplified by ignoring the resistance to heat transfer from the catalyst surface to the gas phase, and the catalyst surface and gas phase are assumed to be at the same temperature. On this basis then, the overall heat transfer coefficients for the fixed-bed and tube-wall reactors are, respectively:

$$U_{\text{fixed bed}} = \frac{1}{\frac{1}{h_o} + \frac{t}{K_t} + \frac{1}{h_s}} \qquad (9)$$

$$U_{\text{tube wall}} = \frac{1}{\frac{1}{h_o} + \frac{t}{K_t} + \frac{c}{K_c}} \qquad (10)$$

For the fixed-bed system, the overall heat transfer coefficient becomes equal to the reactant side film resistance, i.e., $U_{\text{fixed bed}} = h_s$ because the coolant film resistance and metal resistance are insignificant compared to the reactant side film resistance.

The values used for h_o, K_t, and K_c were assumed constant and were equal to 300 Btu/hr-ft^2-°F, 34.6 Btu/hr-ft-°F, and 34.6 Btu/hr-ft-°F, respectively. The value for h_o was based on Dowtherm as coolant, while the values for K_t and K_c were based on iron. However, h_s is dependent on reactant properties. The equation used to calculate h_s came from McAdams "Heat Transmission" (44), with the modification suggested by Smith to allow for the effect of catalyst in the tubes:

$$h_s = \frac{0.023 \times C_{pb}\, G}{\left(\frac{DG}{\mu_f}\right)^{0.2} \left(\frac{C_p \mu}{k}\right)^{2/3}} \times 6 \qquad (11)$$

where:

DG/μ_f = Reynolds Number

$C_p\mu/k$ = Prandtl Number

G = Mass flux

C_{pb} = Heat Capacity

4.2.1.6 Integration

Franks in his book titled "Modeling and Simulation in Chemical Engineering" (45) describes the integration routines exactly as they were used in all three reactor models. Three methods of integration are available within Frank's INT subroutine. These include a first-order method, simple Euler; a second-order method, modified Euler; and a fourth-order method, Runga-Kutta. The fourth-order method was never used.

4.2.2 Reactor Module

More than any other module, the reactor module delineates the differences between reactor systems. This is done in terms of the heat and weight balance equations, and in terms of how the equations are manipulated to arrive at a final solution. Each system will be described separately below.

4.2.2.1 Tube-Wall Reactor

As has already been described, the tube-wall reactor is basically a heat exchanger. It can be schematically represented by Figure 4.2-2. The assumptions made in the development of the model were as follows:

1. Gas flows in ideal plug flow through the reactor.

2. There are no mass transfer limitations in the gas phase.

3. The gas phase and the catalyst are at the same temperature.

The mass balance which resulted from these assumptions and from the rate expressions derived in the Mechanism Sections of this report is as follows:

$$\sum_{i=1}^{N_C} \frac{d M_i}{d X} = \sum_{i=1}^{N_C} \sum_{j=1}^{NR} S_{ij} \cdot r_j \cdot A \qquad (12)$$

The stoichiometric matrix, S_{ij}, controls the stoichiometric relationship between products and reactants. Table 4.2-1 describes the form used for i = 63 components and j = 60 reactions.

The basic heat balance is as follows:

$$\left(\sum_{i=1}^{N_C} M_i \cdot Cp_i\right)\frac{d\,T}{d\,X} = N_T\,\pi\,(D) \cdot U(T_W - T) - A\sum_{j=1}^{NR}(r_j \cdot H_{Rj}) \qquad (13)$$

r_j and H_{Rj} are based on one mole of CO.

From left to right in Equation 13, the terms can be characterized as the specific heat term, the heat removal term, and the heat of reaction term, respectively.

The tube-wall reactor model can be used with the reaction occurring on either the shell side or the tube side of the heat exchanger. The diameter in the heat removal term is equal to the inside diameter of the tube, if the reaction is on the tube side. If the reaction is on the shell side, it is equal to the outside diameter, including catalyst thickness.

4.2.2.2 Entrained Bed Reactor

The entrained bed reactor, as described earlier, is a fast fluidized reactor divided into five sections. Three of these sections are open reactors where the only heat removed is through heat loss to the atmosphere. The other two sections remove heat by exchange with either an oil coolant or steam. As a result, part of the entrained bed reactor module is devoted to identifying, during the integration, the section being calculated.

A schematic representation of the reactor can be found in Figure 4.2-3. The assumptions made in the development of the model were as follows:

1. Catalyst and gas move in an ideal plug flow.

2. There is perfect contacting between solids and gas.

3. There are no mass transfer limitations either in the gas phase or within the catalyst particles.

The mass balance resulting from these assumptions is identical to Equation 12. The only clarification required is on the cross sectional area. In the heat removal sections, the total area is calculated by determining the cross-sectional area of a single exchanger tube and multiplying by the number of tubes. In all other sections, the area is determined by using the inside diameter of the reactor.

The heat balance is as follows:

$$\left(\sum_{i=1}^{N_C} (M_i C_{Pi}) + W_S C_{Ps}\right)\frac{d T}{d X} = N_T \pi (D)\cdot U\cdot(T_W-T) - A \sum_{j=1}^{NR} (r_j \cdot H_{Rj}) \quad (14)$$

The two differences between Equations 13 and 14 are the incorporation of solids in the specific heat term and the manner in which the heat removal term is calculated. In the case of no heat removal, the number of tubes, N_T, is unity and D is equal to the diameter of the reactor. The overall heat transfer coefficient, U, is calculated assuming an insulated wall, and the wall temperature, T_W, is held constant.

In the case of heat removal with an oil coolant, N_T is provided and D is equal to the inside diameter of a tube. U is calculated assuming bare tubes, T_W is set equal to the coolant temperature and is recalculated in each integral interval ΔX. First the total heat removed is calculated for the interval by the equation:

$$Q_L = N_T \pi (D) \cdot U \cdot (T_W - T) \cdot \Delta X \quad (15)$$

The temperature increase of the coolant resulting from absorbing Q_L is calculated by:

$$\Delta T = \frac{Q_L}{M_o C_{Po}} = T_{W_{New}} - T_{W_{Old}} \qquad (16)$$

$T_{W_{New}}$ is then used as the coolant temperature for the next interval ΔX.

When steam is used as a coolant, the wall temperature is assumed constant and dependent on the steam pressure desired.

4.2.2.3 Slurry Reactor

In comparison to the tube-wall and entrained bed reactors, heat transfer is not a problem in the slurry reactor model. The system is assumed isothermal, since cooling coils are immersed in the reaction medium. However, because of the three phase nature of the slurry reactor, fundamental decisions with regard to phase equilibrium, potential mass transfer limitations, and solids distribution are required. The slurry system, as it reflects these decisions, can be schematically represented by Figure 4.2-4. The assumptions involved are as follows:

1. Liquid is completely back-mixed.

2. The system is isothermal.

3. Gas moves in ideal plug flow.

4. All reactions take place in the liquid phase.

5. Solids are evenly dispersed in the liquid phase.

6. Mass transfer limitations only exist in the liquid phase from the gas-bubble interface to the bulk liquid.

7. Gas and liquid are at equilibrium at the gas-liquid interface.

The overall rate of reaction, as implied by these assumptions, is predominately limited by mass transfer from gas bubbles to bulk liquid and by intrinsic kinetics. The mass transfer limiting portion of the mass balance equation has been described by Satterfield and Huff (46) for H_2 as follows:

$$-U_G \frac{dC_{H,G}}{dZ} = k_{L,H}\, a\, (C_{H,L}^* - C_{H,L}) \qquad (17)$$

where:

U_G = superficial gas velocity (cm^3/cm^2 - sec)

$C_{H,G}$ = concentration of hydrogen in gas phase (g moles/cm^3 gas)

Z = vertical distance measured from reactor entrance (cm)

$k_{L,H}$ = liquid film mass transfer coefficient for hydrogen (cm^3 liquid/cm^2 gas-bubble surface area - sec)

a = interfacial area of gas bubbles (cm^2 bubble surface area/cm^3 expanding liquid)

$C_{H,L}^*$ = concentration at equilibrium with the gas

$C_{H,L}$ = concentration in the liquid phase (g moles/cm^3 liquid)

This equation implies that the gas superficial velocity is constant through the reactor system. Although this was a necessary simplification for the analysis performed by Satterfield and Huff, it is not a rigorous solution to the problem. Indeed, the gas volume can contract as much as 50% through the system. Correcting Equation 17 and slightly changing nomenclature leads to the following equation:

$$\frac{-1}{A}\frac{d(V_G Y_i)}{dZ} = k_{L,i}\, a\, C_L \left(\frac{Y_i}{K_i} - X_{bi}\right) \qquad (18)$$

This equation can be further simplified by taking advantage of the fact that:

1. $$\frac{d(V_G Y_i)}{dZ} = V_G \frac{dY_i}{dZ} + Y_i \frac{dV_G}{dZ}$$

2. $$\sum_{i=1}^{n} \frac{dY_i}{dZ} = 0$$

3. $$\sum_{i=1}^{n} Y_i = 1$$

Equation 18 can now be separated into the following two differential equations (Derivation in Appendix D):

$$\frac{dV_G}{dZ} = -A\, C_L \sum_{i=1}^{n} k_{L,i}\, a \left(\frac{Y_i}{K_i} - X_{bi}\right) \qquad (19)$$

$$\frac{dY_i}{dZ} = \frac{AC_L Y_i}{V_G} \sum_{i=1}^{n} \left[k_{L,i}\, a \left(\frac{Y_i}{K_i} - X_{bi}\right)\right] - \frac{AC_L}{V_G} k_{Li,a}\left(\frac{Y_i}{K_i} - X_{bi}\right) \qquad (20)$$

If the values of A, C_L, $k_{L,i}$, a, K_i, and X_{bi} are known, these equations can be integrated through the reactor, and a product rate and composition determined. Values of K_i and A are known when reactor operating conditions and design are set. Zaidi, et al. (47) and Koelbel (48) have reported a value for the interfacial surface area, a, of 305 ft^2/ft^3.

Zaidi, et al. have also reported values for the liquid film mass transfer coefficient, $k_{L,i}$, for CO in molten paraffin on the order of 2.36 ft/hr. The values of $k_{L,i}$ for other components were developed as follows.

Calderbank and Moo-Young (49) have developed an equation which describes the value of k_L as:

$$k_L = 0.31\left(\frac{D_L}{\nu_L}\right)^{2/3} \frac{U_L \Delta \rho_L g^{1/3}}{\rho_L^2} \qquad (21)$$

where:

D_L = diffusivity in the continuous phase

ν_L = kinematic viscosity of the continuous phase

U_L = continuous phase viscosity

$\Delta \rho_L$ = difference in density between dispersed and continuous phases

ρ_L = continuous phase density

g = acceleration due to gravity

If the slurry reactor is at steady state, the values for ν_L, U_L, $\Delta \rho_L$, ρ_L, and g will be roughly constant. The equation can then be rewritten as:

$$k_L = \text{Constant} \times D_L^{2/3} \qquad (22)$$

Wilke and Chang (50) have described the diffusivity of solute A in solvent B as:

$$D_{AB} = 7.4 \times 10^{-8} \frac{T_a(\psi_B M_B)^{1/2}}{u\, V_A^{0.6}} \qquad (23)$$

where:

$\psi_B \cong 1.0$ for hyrocarbons

M_B = molecular weight

T_a = absolute temperature

μ = viscosity of solution

V_A = molar volume of solute as liquid at its normal boiling point

Since ψ_B, M_B, T_a, and μ are constant for a given solvent, the diffusivity can be rewritten as:

$$D_{AB} = \text{Constant} \frac{1}{V_A^{0.6}} \tag{24}$$

If Equations 22 and 24 are combined, the resulting equation is:

$$k_{L_A} = \text{Constant} \frac{1}{V_A^{0.4}} \tag{25}$$

This relation suggests that if the value for the mass transfer coefficient for one component in a given liquid is known, e.g., CO, the mass transfer coefficient of a second component can be estimated by knowing the ratio of the liquid molar volumes of these two components. It is recognized that this is a gross approximation. However, due to a lack of data on k_L values for hydrocarbons and due to a desire for internal consistency, the above method was used for determining k_L values for all components relative to CO.

X_b is the only parameter remaining to be known before integration of the mass transfer mass balance equation can be performed. X_b, however, is also intimately tied to the intrinsic kinetics of the slurry system as described by the mass balance equation:

$$\sum_{i=1}^{NC} \frac{1}{A}\frac{dM_i}{dZ} = \sum_{i=1}^{NC}\sum_{j=1}^{NR} S_{ij} \cdot r_j\,(X_{b_i}) \qquad (26)$$

or for a completely back-mixed system:

$$\sum_{i=1}^{NC} \frac{1}{A}\frac{(M_{i_f} - M_{i_o})}{L} = \sum_{i=1}^{NC}\sum_{j=1}^{NR} S_{ij} \cdot r_j(X_{b_i}) \qquad (27)$$

Since the rate of mass transfer must equal the rate of reaction, the following relationship must be true from Equations 18 and 27:

$$M_{i_f} - M_{i_o} = k_{L_i} \cdot a\, C_L A \int_0^L \left(\frac{Y_i}{K_i} - X_{b_i}\right) dZ = A \cdot L \sum_{i=1}^{NC}\sum_{j=1}^{NR} S_{ij} \cdot r_j(X_{b_i})$$

The key to the solution of the slurry mass balance equations is in choosing values of X_b such that the above equalities are fulfilled.

The heat balance equation for the slurry system is very straightforward. In order for the reactor to be isothermal, any heat generated by reaction must be removed by heat removal. Therefore:

$$Q_L = A \cdot L \cdot \sum_{j=1}^{NR} (r_j \cdot H_{R_j}) \qquad (28)$$

4.2.3 Program Capabilities

The program capabilities are best described in outline form below:

I. Tubular Reactor Model

A. Reactor Configuration

1. Fixed Bed

The catalyst and reaction are on the tube side of the exchanger with the coolant on the shell side.

2. Tube-Wall -- Tube Side

The catalyst is flame-sprayed to the inside of the tubes with the reaction taking place in the tubes. The coolant is in the shell.

3. Tube-Wall -- Shell Side

The catalyst is flame-sprayed to the outside of the tubes and reaction is on the shell side of the exchanger. The coolant is in the tubes.

B. Temperature Control

1. Isothermal

The temperature is fixed and the heat removed is assumed to exactly balance the heat generated by reaction.

2. Adiabatic

No heat is removed and the temperature is allowed to rise with the heat generated by reaction.

3. Non-adiabatic

The temperature is calculated by balancing the heat removed via coolant against the heat generated by reaction.

C. Coolant Type

1. Boiling Dowtherm

2. Boiling Water

In both these cases, "boiling" implies an excess of coolant at constant temperature.

II. Entrained Bed Reactor Model

A. Reactor Configuration

1. Fast Fluidized

One requirement of a fast fluidized bed is that gas move in plug flow. A dense fluidized bed is characterized by back-mixed gas and the model is, therefore, not applicable to this case.

B. Temperature Control

1. Isothermal

2. Non-adiabatic

C. Heat Removal

1. Coolant Type

A. Boiling Water

B. Oil

The oil is not boiling. The increase in oil temperature is calculated based on heat removed from the reaction system.

2. Exchanger Length

In the entrained bed reactor, heat removal does not occur through the entire length of the reactor. Two separate exchanger sections are provided, the lengths of which are variable.

III. Slurry Reactor Model

A. Reactor Configuration

The slurry model uses as basic assumptions back-mixed liquid and plug flow gas. It is not applicable to any other configuration.

B. Temperature Control

1. Isothermal only.

C. Mass Transfer

Mass transfer limitations are only considered from the liquid interface to the bulk liquid. No other mass transfer limitations are considered. Mass transfer coefficients are easily changed.

IV. Capabilities Common to All Reactor Systems

A. Changes can be conveniently made in:

1. Reactor Dimensions
2. Catalyst Concentration
3. Catalyst Rate Constants
4. Operating Conditions

B. Fit versus Predict

The programs can input operating conditions and yield data, and calculate kinetic rate constants which best "fit" the data. Or, the program can input feed composition, operating conditions and kinetic rate constants and "predict" product yields.

C. Kinetic Mechanism

Because of the modular approach used for modeling, new kinetic mechanisms can be easily incorporated into the programs.

FIGURE 4.2-1

REACTOR MODELING MODULAR DIAGRAM

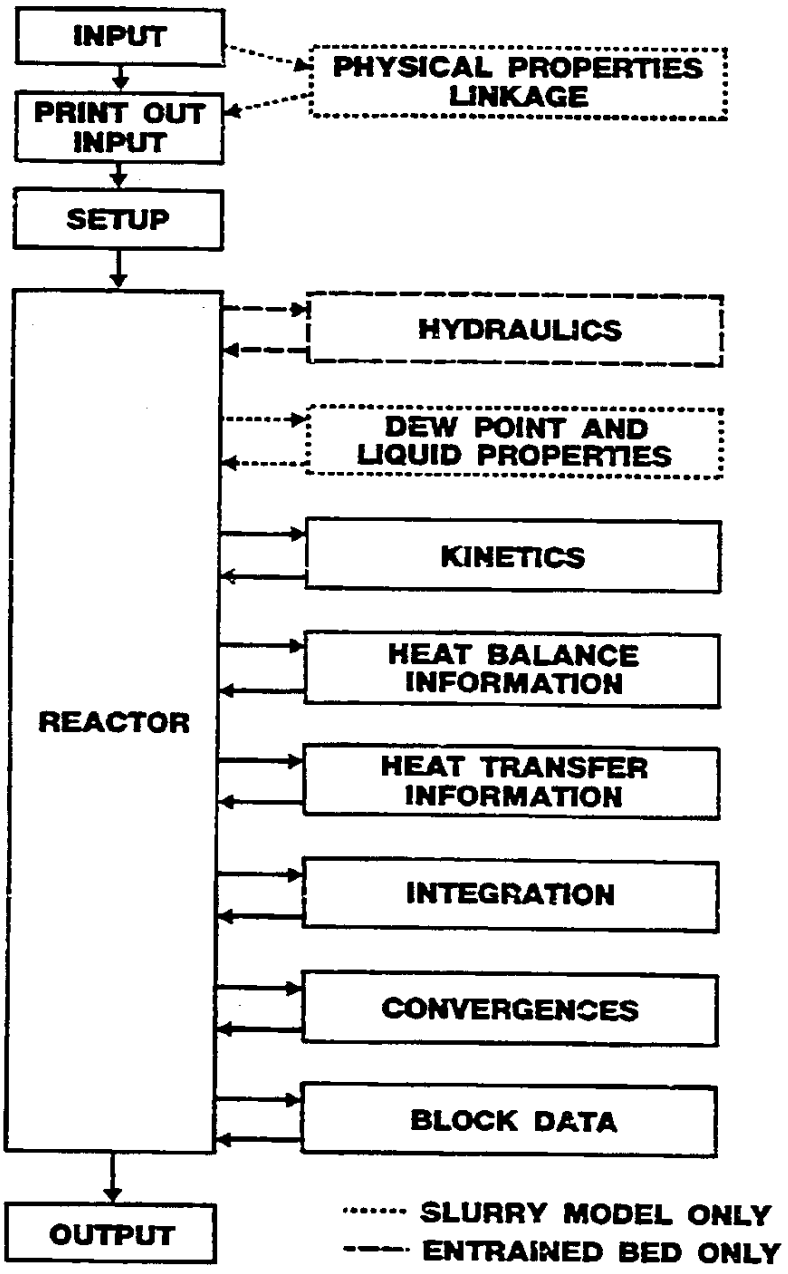

UOP 573-52

FIGURE 4.2-2

SCHEMATIC OF TUBE WALL REACTOR

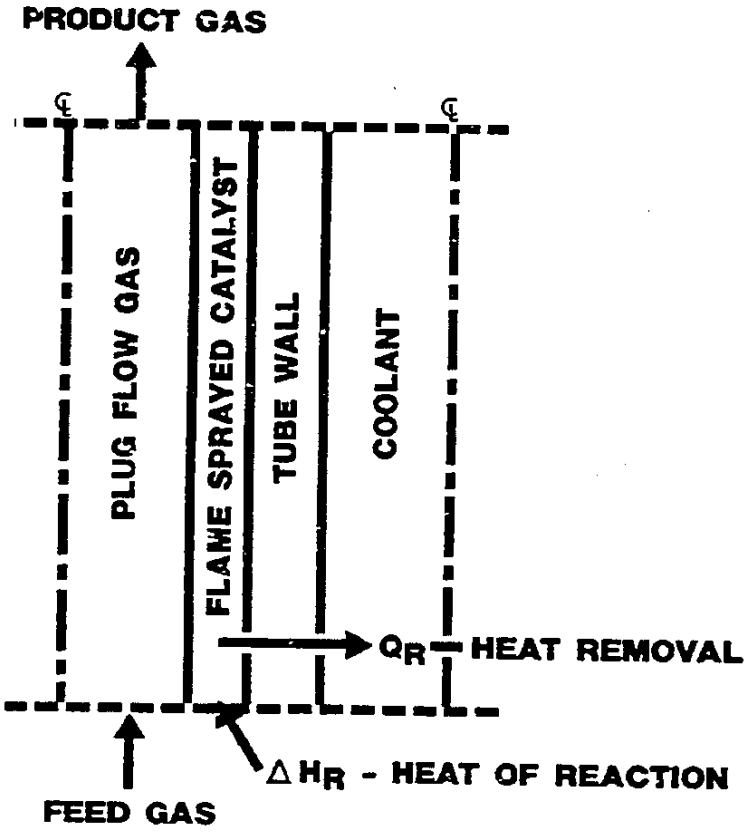

UOP 573-54

FIGURE 4.2-3
SCHEMATIC OF ENTRAINED BED REACTOR

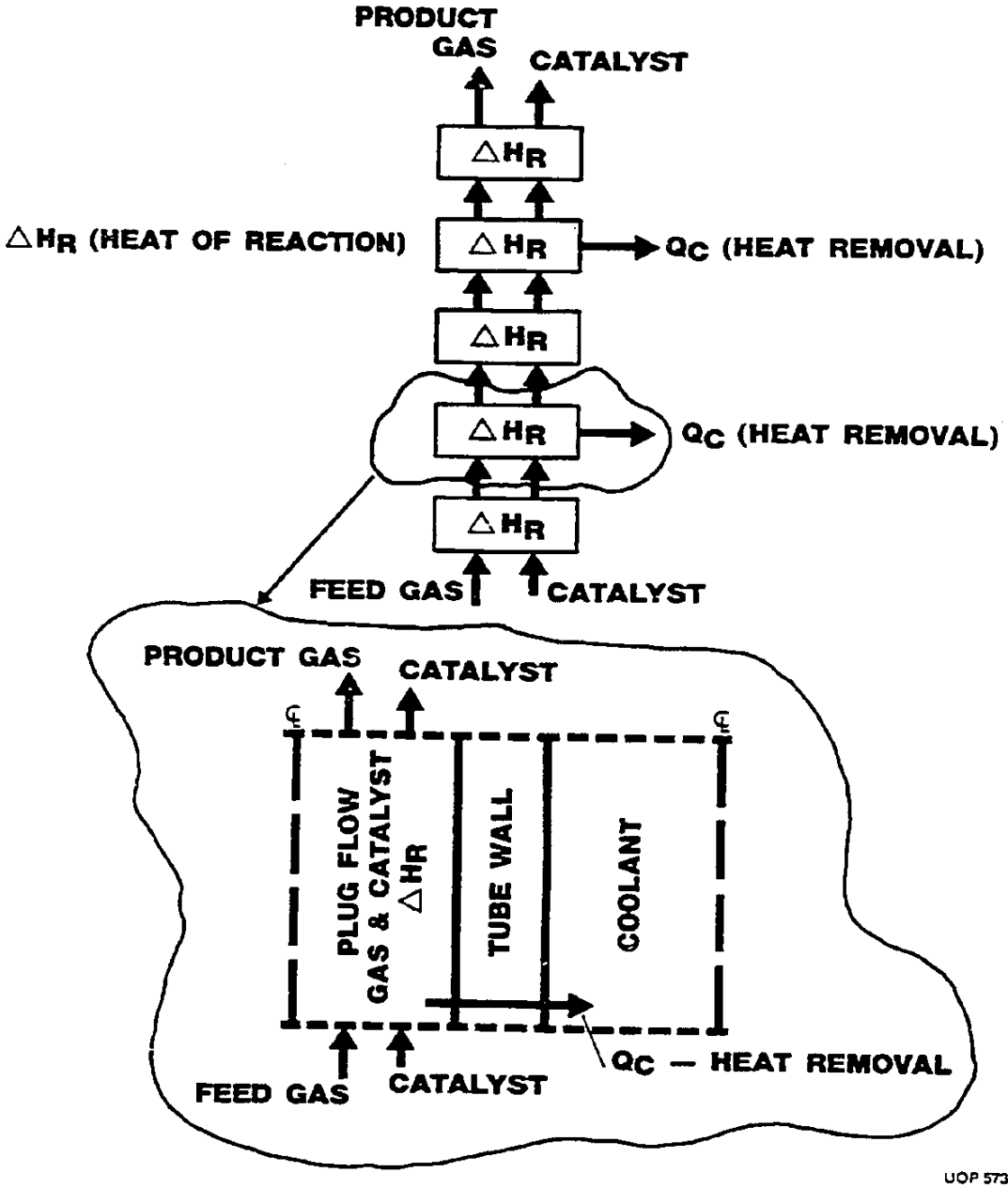

UOP 573-53

FIGURE 4.2-4

SCHEMATIC OF SLURRY REACTOR

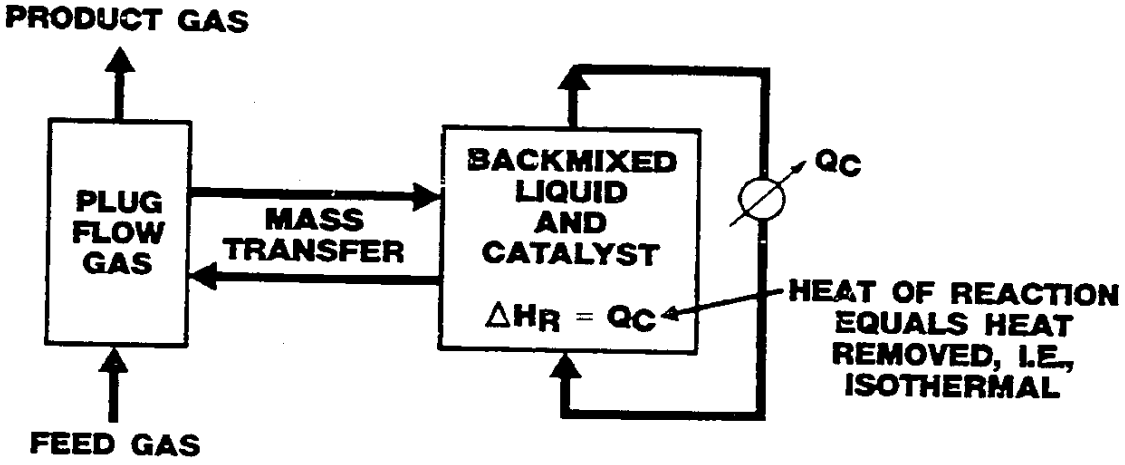

MASS TRANSFER

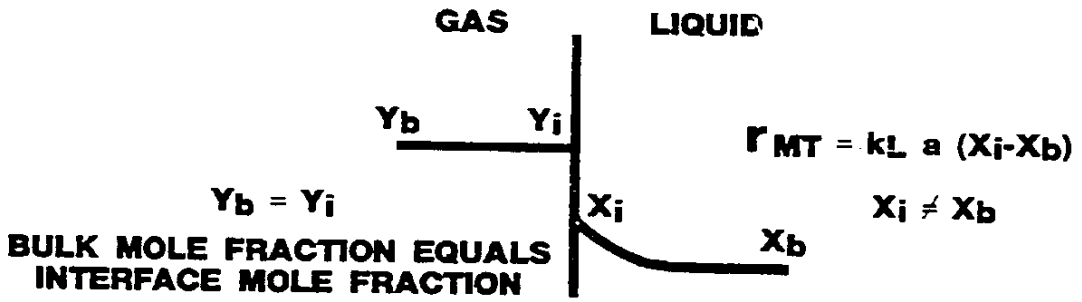

$$Y_i = K_i x_i$$

VAPOR AND LIQUID ARE AT EQUILIBRIUM AT THE INTERFACE

UOP 573-55

TABLE 4.2-1

STOICHIOMETRIC MATRIX

Reaction	i = Component j =	1 H_2O	2 H_2	3 CO	4 CO_2	5 CH_4	6 C_2H_6	7 . . . 34 C_3H_8 . . . $C_{30}H_{62}$	35 C_2H_4	36 C_3H_6	37 . . . 63 C_4H_8 . . . $C_{30}H_{60}$
CH_4	1	+1	-3	-1	0	+1	0	0	0	0	0
C_2H_6	2	+2	-5	-2	0	0	+1	0	0	0	0
C_3H_8	3	+3	-7	-3	0	0	0	+1	0	0	0
$C_{30}H_{62}$	30	+30	-61	-30	0	0	0	0	0	0	0
C_2H_4	31	+2	-4	-2	0	0	0	0	+1	0	0
C_3H_6	32	+3	-6	-3	0	0	0	0	0	+1	0
C_4H_8	33	+4	-8	-4	0	0	0	0	0	0	+1
$C_{30}H_{60}$	59	+30	-60	-30	0	0	0	0	0	0	0
Water Gas	60	-1	+1	-1	+1	0	0	0	0	0	0

4.3 DISCUSSION OF RESULTS

4.3.1 Data Fitting

4.3.1.1 Data Fitting Procedures

The reliability of the mechanism was tested by fitting rate constants to data from all three reactors.

The first step in the data fitting procedure was to identify the variables to be fit. The assumption in the mechanism that each of the rate constants is a constant function for all carbon numbers results in the product distribution being dependent on three rate constants and an equilibrium constant. These are the polymerization rate constant, k_p, the hydrogenation rate constant, k_H, the forward rate constant for the olefin formation, k_o, and its corresponding equilibrium constant, K_e. These are the independent variables in the kinetic mechanism.

The next step was to characterize the product distribution using four corresponding dependent variables. Three of the four became obvious choices. An overall carbon balance of the system could be represented by CO conversion. The distribution of these carbons in the product could be approximated by the degree of polymerization as calculated from a plot of $\ln X_n$ vs. n. (The slope was determined from the gasoline fraction, i.e., between carbon numbers 5 and 11.) The hydrogen balance could be represented either by hydrogen conversion or, since only olefins and paraffins are produced as products, by olefin-to-paraffin ratio. Unless one is willing to consider variations in rate constant or olefin-to-paraffin ratio with carbon number, the three variables mentioned above describe the product in its entirety. From considerations of availability of consistent experimental data, and the desire to use the simplest possible approach in this first modeling attempt, the number of dependent variables has been limited to these three. Unfortunately, trying to fit four independent variables with three dependent variables leads to an infinite number of solutions.

A variable study was, therefore, undertaken to determine if the product distribution was sufficiently insensitive to one of the independent variables to be set equal to a constant. This would reduce the problem to an equal number of independent and dependent variables, thus leading to a unique solution. This study was done in an ideal plug flow reactor under isothermal conditions. A typical result for a given set of rate constants is represented in Figure 4.3-1. Two results of the constraints imposed on the mechanism are reflected in this plot. The first is in the methane production. Both the olefins and the paraffins, individually, are represented as straight lines and, therefore, follow a Schulz-Flory relationship. However, since there is no olefin of carbon number unity, methane can not follow a Schulz-Flory relationship relative to the total carbon number distribution, i.e., sum of the olefins and paraffins.

The second result is the olefin-to-paraffin ratio. Weitkamp, et al. (51), have shown that, for an iron catalyst operating in a fluidized bed, the olefin-to-paraffin ratio remains approximately constant beyond carbon number five. This implies that the olefin and paraffin lines in Figure 4.3-1 are parallel. Although this appears to be the case, in fact, the lines are gradually converging and the olefin-to-paraffin ratio is continually decreasing with carbon number. Later runs with back-mixed reactors did show a constant olefin-to-paraffin ratio above a carbon number of 10 and only a small decrease above a carbon number of 5. At the present time it is not certain whether predictions of olefin-to-paraffin ratio with the proposed mechanism are meaningful, or whether some variation of rate constants with carbon number will be necessary.

Figure 4.3-2 represents the results when, for a given set of k_p, k_H, and k_O values, the value of K_e was changed from low to high. The curvature of the olefin line is caused by the light olefins approaching their respective equilibrium values. This variance from the idealized Schulz-Flory distribution was not the original objective of the mechanism. Although the intent is not to minimize the importance of this approach to equilibrium, as a first approach to the problem the value of K_e has been arbitrarily fixed at a low value for the remainder of our work, so as to more closely approximate the Schulz-Flory distribution of products. After

a value for K_e is imposed, the overall problem of fitting is reduced to three dependent variables and three independent variables and can be readily solved.

In addition to limiting the number of independent variables, the variable study provided information regarding the relative sensitivity of CO conversion, degree of polymerization, and olefin-to-paraffin ratio to the three remaining independent variables, k_p, k_o, and k_H (Table 4.3-1). CO conversion is obviously most influenced by k_p and was, therefore, chosen as its fitting parameter. The degree of polymerization and olefin-to-paraffin ratio were affected equally by k_H and k_o. An arbitrary decision was taken to fit k_H to the degree of polymerization and k_o to the olefin-to-paraffin ratio. However, the same results were achieved when the fitting parameters for k_o and k_H were reversed.

The preceding discussion has revolved around three unknown rate constants. Actually each rate constant contains two unknown parameters, i.e., the Arrhenius frequency factor and the activation energy. The Arrhenius equation can be written as:

$$k_T = k_o{}^o e^{-\Delta E/RT_a} \tag{29}$$

For a given catalyst, the frequency factor and the activation energy are fixed and the rate constant varies only as a function of temperature. The values of $k_o{}^o$ and ΔE were determined from the standard Arrhenius plot of ln k_o versus $1/T_a$.

The rate expression for the water-gas shift reaction was given by Equation 8. Since the equilibrium constant is well known, the only variable that needs to be fit is the forward rate constant, k_{WG}. The CO_2 concentration was chosen as the fitting parameter, since for the reaction included in the models the production of CO_2 is unique to the shift reaction.

4.3.1.2 Data Fitting Results

As mentioned in Section 4.3.1.1 of this report, the Arrhenius activation energies were determined by fitting the frequency factors to data at different temperatures. The fitting parameters were CO conversion, degree of polymerization and olefin-to-paraffin ratio.

The tube-wall reactor system was chosen for this work; first, because the simplicity of the plug flow system made results easy to interpret, and, second, because consistent results at different temperatures were not available for the other reactor systems. Table 4.3-2 represents temperature data collected by Haynes, et al., of PETC (11) for the tube-wall reactor operating with flame-sprayed taconite catalyst at 650 psig. The degree of polymerization for each of these sets of data was determined in the following manner:

1. The product was divided into the following components:

   a) C_1-C_4 (gas)
   b) C_5-C_{11} (gasoline)
   c) C_{12}-C_{25} (diesel)
   d) C_{26}+ (heavy)

2. The Schulz-Flory plot of degree of polymerization versus weight fraction shown in Figure 4.3-3 was used to determine which degree of polymerization most nearly approximated the actual data.

The olefin-to-paraffin ratio required special consideration. As mentioned earlier, it remains to be determined whether the mechanism can predict olefin-to-paraffin ratio as a function of carbon number. In order to avoid this problem, an artificial ratio of unity was used in each of the data fitting runs. This in effect reduced the number of independent variables to two, CO conversion and degree of polymerization. However, despite the deficiencies of this first, deliberately simplified approach,

useful insight into the strengths and weaknesses of the various reactor systems was gained. The final information used as input for the tube-wall fitting is given in Table 4.3-3.

The frequency factor results versus temperature as well as the corresponding activation energies are given in Table 4.3-4. The values are based on a reference temperature of 1100°R. As can be seen, excellent agreement in frequency factors was achieved. The largest variance (15.3%) is for the water-gas shift reaction. The smallest variance (2.5%) is for the polymerization rate constant. The activation energies are typical of those for catalyzed reactions.

Because of the limited temperature data available, the above procedure for determining activation energies could not be used for each reactor system. Consequently, the activation energies given in Table 4.3-4 were used without modification for the gas phase reactor systems. In the case of the slurry reactor, Satterfield and Way (52) have shown that for a system where the carrier liquid is completely inert to reaction and/or adsorption on the catalyst site, the liquid phase reaction rate constant can be related to the gas phase reaction rate constant by the following equation:

$$k_L = K \frac{V_G}{V_L} \quad k_G \qquad (30)$$

where:

k_L = liquid phase reaction rate constant

K = vapor-liquid equilibrium constant, $K = \frac{y}{x}$

y = mole fraction in gas

x = mole fraction in liquid

V_G = molar volume of gas at reactor conditions

V_L = molar volume of liquid at reactor conditions

k_G = gas phase reaction rate constant

Equations of this form were incorporated into the slurry mathematical model allowing k_G and the activation energies given in Table 4.3-4 to be used for the slurry system. The relatively good agreement obtained in fitting data for other reactor systems confirms that this is a reasonable assumption.

While the fixed-bed tubular reactor is not one of the reactors to be compared in this study, an abundance of data is available for a reactor of this type developed by the Pittsburgh Energy Technology Center (53, 54), in which lathe turnings were used as catalysts. Since the tube-wall reactor model can also be used for a fixed-bed reactor, a comparison of the catalyst used in these two systems was made. The frequency factor fit for the lathe turning reactor was made on the basis of Experiment 26C of the PETC work (54). (See Table 4.3-5). The comparison is presented in Table 4.3-6.

At first glance, the lathe turnings results look quite different from the tube-wall results. However, upon closer analysis, two explanations emerge. The first is related to catalyst activity. The computer model performs its calculations using weight as its basis for catalyst concentration. Actually, for this catalyst which has very little pore volume, the catalyst activity is more closely related to the external surface area than to the weight. The surface area per unit weight of the lathe turning catalyst was compared to that of the tube-wall catalyst, and was found to be very close to the ratio of the frequency factors for the polymerization and for the water-gas shift rate constants. In other words, the high apparent activity of the lathe turning catalyst could be easily explained by its higher surface area. The polymerization rate constant was, therefore, used as a basis to adjust the frequency factors derived for the lathe turning catalyst to the catalyst surface area in the tube-wall reactor. The adjusted numbers are also shown in Table 4.3-6.

In spite of this adjustment, the agreements between catalysts for the hydrogenation and for the olefin formation frequency factors are still poor. This led to the second explanation. The lathe turning catalyst used for fitting purposes was potassium promoted while the tube-wall

catalyst was not. There is much evidence in the literature (30, 55) that suggests that potassium promotion increases the degree of polymerization of the product. Based on a comparison of frequency factors, this phenomenon might be explained by a reduction in the hydrogenation/termination rate, thereby producing a heavier product via additional polymerization. Weitkamp, et al. (51), have provided support to this theory by showing a significant shift from a paraffinic to olefinic product with the addition of potassium.

Additional support for these explanations is provided when similar comparisons are made for the slurry and entrained bed systems. Koelbel's (7) yields and operating conditions, shown in Table 4.3-7, were used for fitting the slurry system. The Kellogg Feasibility Study (4) was used as a basis for yields and some of the operating conditions for the entrained bed system. In the latter case, however, Sasol literature, as well as engineering judgment, was required to supplement some deficiencies in the available data. The final information used for fitting is given in Table 4.3-8.

Frequency factor derivations are given at the top of Table 4.3-9. Here again the magnitudes of the frequency factors for the polymerization rate constant were found to be roughly in proportion to the catalyst surface areas. For example, the difference between the frequency factors for the slurry and entrained bed reactors could be explained by the average particle size of the catalyst being 30 and 40 microns, respectively. In addition, the surface area per unit weight of catalyst is very high for both these systems, and is reflected in the high frequency factors relative to the tube-wall system.

The bottom of Table 4.3-9 shows the values of frequency factors after adjustment for surface area relative to the tube-wall catalyst. The similarity of values for the lathe turning catalyst and for the slurry catalyst is significant. Both catalysts are potassium promoted and this is reflected in the values for k_H^o and k_O^o. While the entrained bed values are not as close, they are still in reasonable agreement, considering the lack of a consistent set of operating data for fitting. The only

frequency factor that is completely out of line is for the water-gas shift in the entrained bed system. A closer scrutiny of the data revealed a high concentration of CO_2 in the combined feed. As a result, water-gas shift was found to be at equilibrium throughout the entire reactor. It is obviously impossible to determine a forward rate of reaction when that reaction is at equilibrium. This value must, therefore, be disregarded.

The frequency factors used in the entrained bed and slurry variable studies are those listed at the top of Table 4.3-9. These produced the most favorable yield structures for their respective reactor systems. The tube-wall frequency factors, however, produced yield structures that were much too high in methane yield and much too low in gasoline yield. Conversely, the lathe turning values, although better, produced a product structure that was too heavy. A compromise led to the final selection of the lathe turning values modified for slightly less potassium promotion. This was accomplished by increasing the hydrogenation frequency factor from 0.07 to 0.1. The values used were: $k_p^o = 73.0$; $k_H^o = 0.1$; $k_o^o = 0.0129$; and $k_{WG}^o = 205.0$.

A very important overall conclusion was drawn from reflecting on the data fitting results. That is, a single mathematical mechanism has been developed that, when incorporated into models of three completely different reactor systems operating at completely different operating conditions, gave reasonable agreement on the rate constants associated with Fischer-Tropsch catalysts manufactured by several independent investigators. Also, the data with and without potassium promotion of the catalyst show that the mechanism will allow interpretation of yield differences resulting from different catalyst formulations. The reactor comparisons, therefore, proceeded with some confidence that the models also can be used to predict with reasonable accuracy the gross product distributions for each system.

4.3.2 Parsons Comparison

Under DOE Contract No. E(49-18)-1775, Ralph M. Parsons Company (16) prepared a report which describes "The results of a conceptual design and

economic evaluation for a conceptual Fischer-Tropsch plant responsive to U.S. demands and economic requirements." The Fischer-Tropsch synthesis reactor chosen for this study was the tube-wall system. The yield structure was based on Experiment 26C (Table 4.3-5) with the lathe turning catalyst mentioned earlier. The activity of the catalyst was determined from Experiment HGR-34 (Table 4.3-10) which studied flame-sprayed magnetite. The final design selected by Parsons is given in Table 4.3-11. A comparison of this conceptual design with the PETC experimental data is given in Table 4.3-12. A critical analysis suggests that the activity selected for the conceptual design was very optimistic. The fit results presented in Table 4.3-6 earlier suggested that the polymerization activity, k_p^o, of lathe catalyst is very nearly the same as that for flame-sprayed taconite catalyst. Haynes, et al. (1), have shown that taconite catalyst is significantly less active than magnetite catalyst and yields a higher molecular weight product. Closer examination of Experiments 26C and HGR-34 shows that potassium-promoted magnetite has a much lighter product structure than potassium-promoted lathe turnings. Potassium-promoted taconite must, therefore, be used as catalyst if the lathe turning yield structure represented in the Parsons study is desired.

A study was undertaken to compare the Parsons reactor design and operating conditions, which were based on flame-sprayed magnetite, to that which would result from a flame-sprayed, potassium-promoted taconite (or lathe turning equivalent). The results are given in Table 4.3-13. Case 1 used the Parsons reactor design. (The GHSV is not quite the same, but this is the result of using bare tubes in the model while Parsons used finned tubes.) The lower activity and heavy product distribution of the taconite catalyst is reflected in a low CO conversion and a high degree of polymerization. In Case 2, the temperature was increased to 640°F and the size of the reactor was increased until a CO conversion on the fresh feed of 90% was achieved. The predicted yields are then close to what was used in the Parsons study, but the total syngas conversion ($CO + H_2$) remains lower than that used by Parsons, and the reactor is roughly twice the size with an operating temperature considerably higher.

This study is presented as an example of how the reactor models can be used to interpret experimental data and predict the results of using commercial-scale equipment. The design shown in Table 4.3-13 is not represented as an optimized design for a tube-wall reactor. In fact, it is doubtful that this reactor could operate at 640°F and the H_2/CO ratio indicated without significant problems of free carbon formation.

4.3.3 Variable Studies

4.3.3.1 Tube-Wall Reactor

The base case operating conditions chosen for the tube-wall reactor variable studies were as follows:

Gas	:	Once-through
Temperature	:	310°C (589°F)
Pressure	:	415 psia
J Factor	:	5 SCFH FF/ft^2 catalyst
H_2/CO Ratio	:	2.0
Catalyst Density	:	11.85 lb/ft^3 of reactor.

These are not necessarily the optimum operating conditions for this reactor system. They were chosen so the sensitivity to CO conversion and degree of polymerization could be properly shown as a function of various parameter changes.

Figures 4.3-4 through 4.3-6 show CO conversion versus reactor temperature as functions of pressure, J factor, and inlet H_2/CO ratio, respectively. In general, conversion is found to increase almost linearly with increasing temperature until high conversions (> 90%) are reached. At this point there is an exponential approach to 100% conversion. At a given temperature, conversion is found to increase with increasing pressure, decreasing J factor, and increasing H_2/CO ratio.

Figures 4.3-7 through 4.3-9 give degree of polymerization versus reactor temperature as functions of pressure, J factor, and H_2/CO ratio,

respectively. In agreement with the literature, DP decreases with increasing temperature. At a fixed temperature, DP increases with increasing pressure, increasing J factor, and decreasing H_2/CO ratio.

The H_2/CO ratio information presented in Figure 4.3-9 is represented in another form in Figure 4.3-10. Here, degree of polymerization is plotted versus CO conversion at varying inlet H_2/CO ratios. Notice that with a single reactor configuration and at a fixed conversion there is a maximum degree of polymerization at a H_2/CO ratio near unity. This is explained as follows. As H_2/CO ratio decreases, conversion decreases with a corresponding increase in the degree of polymerization. To return the conversion to its original value, it is necessary to increase temperature which decreases DP. At a H_2/CO ratio of 0.7, the temperature effect on degree of polymerization dominates the H_2/CO ratio effect, while the opposite is true at a H_2/CO ratio of 2.0.

A second influence of H_2/CO ratio on degree of polymerization can be seen in the plot of DP versus temperature at varying recycle-to-feed ratios (Figure 4.3-11). Initially it was felt that increasing the recycle ratio would increase olefin concentration in the combined feed and, therefore, encourage propagation to heavier products (higher DP). Inspection of Table 4.3-14 shows that the olefin concentration does increase modestly, but the hydrogen and carbon monoxide concentrations remain an order of magnitude higher and, therefore, continue to be the dominant factors in determining the degree of polymerization.

This dominance can be seen more clearly when one understands the severe effects of recycle ratio on degree of polymerization at low temperature versus at high temperature (Figure 4.3-11). Two temperatures, i.e., 539 and 615°F, were chosen for monitoring, at different recycle ratios, the H_2 and CO concentrations and the degree of polymerization as a function of reactor length. Figures 4.3-12 and 4.3-13 represent the concentration changes while Figures 4.3-14 and 4.3-15 represent the degree of polymerization changes.

At 539°F, the CO conversion is rather low. The concentrations of both H_2 and CO, therefore, remain relatively high throughout the reactor length. The influence of these concentrations on both termination and polymerization is such that the degree of polymerization decreases almost linearly with reactor length. As the recycle ratio is lowered, the change in H_2/CO ratio becomes higher, thus accelerating the decline in degree of polymerization. Near the end of the reactor, the lines cross and a lower degree of polymerization is seen for the lowest recycle ratio.

At 615°F, the CO conversion is rather high. Although the concentration of H_2 remains relatively high, the concentration of CO begins to level off at a low value, particularly for R/F = 0. As a result, the influence of CO on the rate of polymerization ($r_p \cong k_p[CO][H_2]$) becomes minor, and the rates of termination ($r_t \cong k_H [H_2]$) and polymerization become dependent on the hydrogen concentration alone. As can be seen in Figure 4.3-15, the net effect is a leveling out of degree of polymerization with reactor length. The recycle ratio lines never cross, and the degree of polymerization for R/F = 0 remains the highest throughout the reactor.

4.3.3.2 Entrained Bed Reactor

Because of the complexity of the entrained bed system, the effect of a single variable change is difficult to study. For example, the definition of reactor temperature is a problem due to the nature of the heat removal system. Given a fixed inlet temperature, the outlet temperature, and consequently the average reactor temperature, could be changed by adjusting the cooling oil rate to the heat removal coils. An illustration of the models prediction of this effect on CO conversion and degree of polymerization can be seen in Figures 4.3-16 and 4.3-17. As cooling oil rate is reduced, reactor ΔT increases, resulting in an increased conversion and decreased degree of polymerization.

The limited flexibility inherent to the entrained bed reactor system created another example of the difficulty in changing a single variable. An attempt was made to reduce the recycle ratio to below one. When this

was done, the partial pressures of both hydrogen and carbon monoxide in the combined feed increased. In addition, the superficial velocity in the reactor was reduced resulting in increased residence time and higher catalyst concentrations. The net result was a temperature runaway before the first set of exchangers was reached.

These types of complexities led to two guidelines for conducting variable studies on the Kellogg design:

1. A constant ΔT across the reactor was maintained by adjusting cooling oil rate equally between the two heat removal sections, and

2. The rate and composition of hydrocarbons in the recycle gas were held constant and equal to that shown by Kellogg.

With these guidelines, CO conversion and degree of polymerization were investigated as functions of inlet temperature, inlet pressure, β (defined as standard cubic feet of fresh feed per hour per pound of catalyst), catalyst circulation rate, and H_2/CO ratio in the combined feed. Figures 4.3-18 to 4.3-22 represent the results.

As expected, increasing temperature and H_2/CO ratio leads to increasing conversion and decreasing degree of polymerization. Increasing pressure increases both CO conversion and the degree of polymerization.

The influence of catalyst circulation rate is unique to the entrained bed system. Yerushami, et al. (56), have shown that for a fixed gas rate, if the catalyst circulation rate is increased, i.e., the catalyst loading is increased (lbs catalyst per ft^3 of gas), additional slippage will occur resulting in higher catalyst density in the reactor. This effect can be seen in Figure 4.3-23 for the base case. The increased catalyst density leads to higher conversions (Figure 4.3-21), but apparently has little effect on the degree of polymerization.

The influence of solids loading on catalyst density led to the term β, defined above, being chosen as a correlating factor rather than gas

hourly space velocity (GHSV). Although GHSV may be a measure of space utilization efficiency, it is not an accurate measure of catalyst utilization efficiency for the entrained bed reactor. CO conversion decreases dramatically with increasing β (Figure 4.3-20), while degree of polymerization increases only slightly.

The final variable to be studied was recycle to feed ratio. In this case the ΔT guideline was adhered to, but steady state continuous recycle was simulated by continually adjusting recycle gas composition until it matched the gas composition produced from a flash of reactor effluent. The results are presented in Figures 4.3-24 and 4.3-25. As expected, increased recycle to feed ratio results in lower overall CO conversion. The influence of this lower conversion on degree of polymerization can be seen in Figure 4.3-25. From the tube-wall recycle studies (Section 4.1) at low temperatures, it was shown that large changes in CO concentrations relative to H_2 concentrations, characteristic of low conversions, significantly reduce the rate of polymerization relative to the rate of termination. The net result is a lower degree of polymerization at lower recycle-to-feed ratios. At higher temperatures and higher conversions, the final CO concentrations for both recycle cases are low enough that their influence on polymerization relative to each other is insignificant. The corresponding degrees of polymerization are, therefore, approximately equal.

4.3.3.3 Slurry Reactor

In choosing operating conditions for the slurry reactor variable study, sensitivity to parameter changes for both upward and downward directions of perturbation was desired. Koelbel's choice of operating conditions, i.e., low temperature, low pressure, low H_2/CO ratio, and high conversion (Table 4.3-15), limited the sensitivity to CO conversion at elevated pressures. Space velocity was, therefore, increased to reduce CO conversion to roughly 90%. The results of the present study are shown in Figures 4.3-26 and 4.3-27. The effect of a 126 psi increase in pressure on CO conversion is roughly 4% at low temperatures while decreasing to 1.5% at high temperatures. The effect on degree of polymerization, on the other hand, was almost negligible at all temperatures.

GHSV studies were performed at Koelbel's operating pressure, i.e., 174 psia, and can be seen in Figures 4.3-28 and 4.3-29. As expected, CO conversion decreases with increasing space velocity. The degree of polymerization on the other hand increases with increasing space velocity. This is clearly a result of the relative concentrations of CO and H_2 in the reactor at different conversion levels. The influence of CO and H_2 concentrations on degree of polymerization have been discussed in the tube-wall reactor section (Section 4.3.3.1) and will be discussed further in Section 4.3.4. The same arguments apply here.

Figures 4.3-30 and 4.3-31 represent the effects of H_2/CO ratio. H_2/CO ratio has a large influence on the degree of polymerization, while having a smaller effect on CO conversion. Here again, the effect of relative H_2 and CO concentrations on the competition between termination reactions and polymerization reactions is clearly demonstrated.

The question of mass transfer limitations in the slurry reactor has received significant attention in the literature but, to date, has not been answered conclusively. A set of conditions suggested by Koelbel (7) was used to determine the sensitivity of two mass transfer parameters on CO conversion and degree of polymerization. The first parameter, the specific interfacial area, is a measure of the bubble surface area available per volume of reactor space. The second parameter, the mass transfer rate constant, fixes the rate of mass transfer for a given component.

Although some work has been done on determining specific interfacial areas in slurry systems, values reported are at best approximations. The value chosen for the majority of these studies, 305 ft^2/ft^3, is consistent with those reported by Koelbel (2) and Deckwer (57). A study was made to determine the influence of a 20% lower interfacial area. Figures 4.3-32 and 4.3-33 represent results with interfacial surface area of 244 and 305 ft^2/ft^3. A lower interfacial surface area reduces the CO conversion roughly 0.2-0.8%, but does not affect the degree of polymerization. The latter result is not surprising since the interfacial area should influence the rate of mass transfer of all components equally.

In order to study the influence of mass transfer rate on CO conversion and degree of polymerization, the values of the mass transfer rate constant, k_L, for hydrogen and CO were individually adjusted 20% above and below their respective base values. The results are presented in Figure 4.3-34. As can be seen, neither the mass transfer rate constant for H_2 nor the constant for CO has a dramatic effect on either CO conversion or degree of polymerization.

These results do not support the conclusion that the slurry reactor operating at Koelbel's conditions is mass transfer limited.

4.3.3.4 Ebullating Bed Reactor

The ebullating bed reactor is believed to differ from the slurry reactor in two respects, i.e., catalyst particle size and liquid flow characteristics.

Since heat removal is accomplished by a circulating liquid stream, larger particles are used to prevent the catalyst carryover which would normally occur if slurried catalyst was used. However, this size difference also introduces the question of possible mass transfer limitations within the pore structure of the larger particles. Although many similarities exist between an ebullating bed reactor and a slurry reactor, this added complexity prevented the development of an ebullating bed model. However, if one speculates on the influence of pore diffusion, the following results might be drawn:

1. Since, by definition, mass transfer limitations result in lower concentrations of reactants at the catalytic site, conversion per site will be lower for the ebullating bed system than for the slurry system.

2. Throughout Section 4.3, the dependence of product yields on the relative concentrations of H_2 and CO has been illustrated. Since the diffusivity of hydrogen in molten wax is higher than that of CO [Zaidi, Louisi, Ralek, Deckwer, (47)], pore diffusion

limitations will result in a higher H_2/CO ratio at the catalytic site and consequently a lower degree of polymerization could be expected.

Liquid flow characteristics in the ebullating bed reactor are also believed to differ from the slurry reactor. Larger particles not only create concerns about pore diffusion, but large particles also maintain a much more structured order in a flowing environment than do fine particles, thereby restricting back-mixing of the liquid. To observe the influence of restricted back-mixing, the slurry model was run as a two-stage system using the Koelbel reactor as a basis. As one can see from Table 4.3-16, the total CO conversion for the two-stage system is 97% compared to 91% for the single-stage system, and the degrees of polymerization are 5.1 and 4.0, respectively. The first stage in the two-stage system is the primary cause for these differences. In the case of conversion, the H_2 and CO concentrations in the first stage are higher than those in the single stage system. This higher driving force results in a 85% conversion. If a driving force equivalent to the single stage system was used, the conversion would be roughly 53%. The net result is a higher total CO conversion in the two-stage system. In the case of degree of polymerization, the H_2/CO ratio in the first stage is 1.4 compared to 1.8 for the single stage system. Here again the driving force to a higher degree of polymerization is much greater than the equivalent driving force in the single stage system, and the net result reflects this.

4.3.4 Response of Degree of Polymerization to Space Velocity

One puzzling result of the modeling work was the prediction that the degree of polymerization would decrease as the residence time increased. This was true regardless of reactor type and occurred within the entire range of Fischer-Tropsch operating conditions. A polymerization product intuitively becomes heavier the lower the reactor gas hourly space velocity.

The key to understanding this result lies in the competition between polymerization and termination. The longer the growing chain remains at a

catalyst site before being hydrogenated to a paraffin, or leaves the catalyst site as an olefin, the higher the degree of polymerization and the molecular weight of the product. This, therefore, will be a function of the relative rates of these processes.

The polymerization term ($D = k_p [CO] [H_2]$) is a function of the partial pressure of both CO and H_2. The irreversible hydrogenation to paraffins term ($E = k_H [H_2]$) is only a function of hydrogen partial pressure. Because of the water-gas shift reaction, the CO conversion through a reactor is much higher than the hydrogen conversion, resulting in the partial pressure of CO dropping much more across the reactor than that of hydrogen. For example, the volumetric percentage of CO may go from 35% at the inlet to 5% at the outlet, while the hydrogen goes from 65% to 45%. This will result in the polymerization term falling to 10% of that at the inlet while the hydrogenation term is still 70% of that at the inlet. The ratio has, therefore, changed by a factor of 7, and this will cause a falling molecular weight of product and a lower degree of polymerization with increasing conversion.

The other factor that can influence the molecular weight of the product is related to the reversible termination reaction to form olefins. The effect of this reaction is to influence the proportion of CO reacting to initiate new chains compared to that elongating existing chains. As the concentration of olefins in the vapor phase increases, the reverse reaction will slow down the rate of release of olefins to the vapor phase. However, in the investigations carried out to date with the reactor models, two factors combine to make this effect insignificant. First, the concentration of olefins is still quite low at the outlet of the reactor in all cases, because of the high concentrations of H_2, CO_2 and H_2O, which are inherent to the reaction system. (The slurry system has the highest olefin concentration at the outlet, but it is still less than 5 mol-%.) The rate of the reverse reaction, therefore, will be low because of the low olefin concentrations. Second, the value of K_e used in these studies was not determined from experimental data. (The selected value is discussed in Section 4.3.1.) If experimental data support a lower value of K_e (i.e., a higher rate constant for the reverse reaction), this can

increase the influence of this effect. An investigation of the effect of olefin concentration on the degree of polymerization of the product will have to wait for further experimental data.

Table 4.3-17 provides an overall view of what happens with increasing CO conversion. Here the conversion at the reactor outlet is 98.3%. The hydrogen content remains high while the olefins only reach 3 mol-%. The CO concentration decreases from 32 to 1 mol-%.

Another way of understanding this phenomenon is from a purely mathematical point of view. A decreasing degree of polymerization fundamentally means that the rate of formation of a heavy component is less than that of a light component. Or, the rate of formation of a light component divided by that of a heavy component is greater than unity. As an example:

$$\frac{r_{C_2H_6}}{r_{C_3H_8}} > 1 \tag{31}$$

Using the mathematical expressions derived for these rates, one obtains:

$$\frac{r_{C_2H_6}}{r_{C_3H_8}} = \frac{AC + B[C_2H_4]}{A^2C + B \cdot A\,[C_2H_4] + B\,[C_3H_6]} \tag{32}$$

If Equation 32 is rearranged, one obtains:

$$\frac{r_{C_2H_6}}{r_{C_3H_8}} = \frac{1}{A + \dfrac{[C_3H_6]}{\dfrac{AC}{B} + [C_2H_4]}} \tag{33}$$

For this ratio to be greater than unity, the denominator must be less than unity, or:

$$\frac{[C_3H_6]}{\frac{AC}{B} + [C_2H_4]} < 1 - A \qquad (34)$$

Typical magnitudes (Tube Wall Reactor R-29T) of these numbers are as follows:

$$A = 0.504$$

$$\frac{AC}{B} = 8.97 \times 10^{-3}$$

$$[C_3H_6] = 1.0 \times 10^{-6}$$

$$[C_2H_4] = 1.15 \times 10^{-6}$$

Considering the relative magnitude of the olefin concentration terms compared to the value of AC/B, it is apparent that the left side of Equation 34 is less than the right side and, therefore, the degree of polymerization is decreasing through the reactor.

What are the factors required to reverse the trend causing the degree of polymerization to decrease through the reactor? In other words, what is required for the following equation to hold:

$$\frac{[C_3H_6]}{\frac{AC}{B} + [C_2H_4]} > 1 - A \qquad (35)$$

The most obvious factor is for the concentrations of the olefins to increase to an order of magnitude equivalent to, or greater than the value of AC/B. As mentioned earlier, this is unlikely since olefin concentrations always remain extremely low throughout the reactor.

Another possibility lies in the value of A. One notices that as A approaches unity, the right side of Equation 35 approaches zero and at some point will be less than the left side. The definition of A is:

$$A = \frac{k_p[CO][H_2]}{k_p[CO][H_2] + k_H[H_2] + k_o} \tag{36}$$

where terms are defined in Section 4.1. For A to approach unity,

$$k_H\,[H_2] + k_o << k_p\,[CO][H_2] \tag{37}$$

The right and left sides of this equation represent the polymerization rate term and the termination rate terms, respectively. Therefore, as one might expect, polymerization must completely dominate termination in order to have an increasing degree of polymerization through the reactor.

A third possibility lies in the value of B. If B is very large, the value of AC/B will eventually become the same order of magnitude as the olefin concentration terms. B is defined as:

$$B = \frac{k_o}{K_e\,(k_o + k_p[CO][H_2] + k_H\,[H_2])} \tag{38}$$

Since $k_o/(k_p + RI + RT)$ is always less than unity, the only way to make B large is to have K_e very small. This is precisely the conclusion at the beginning of this section.

To this point, the entire discussion has revolved around the mechanism as it was originally derived. It should be pointed out that there were three assumptions made during the derivation that may be influencing the results. The first is the assumption of steady state. In a non-steady state system, it is obviously impossible in a polymerization reaction to make a C_{20} component before a C_{19} component is available. The steady state assumption, on the other hand, suggests that all components are available immediately upon entering the reactor. The rate of production of any given component, therefore, can not be inhibited by the lack of availability of another.

The second is the assumption of fixed rate constants and equilibrium constants for all carbon numbers. Since degree of polymerization is influenced by the rates of formation of components relative to each other, it is apparent how fixed rate constants could restrict this particular yield characteristic.

The third is the assumption with regard to order of the reactions. The polymerization term was assumed to be first order with respect to both hydrogen and carbon monoxide. The paraffin termination term was assumed to be first order with respect to hydrogen only. The olefin termination was assumed to be zero order. If polymerization was found to be zero order with respect to CO, for example, the entire analysis with regard to relative CO and hydrogen concentrations would no longer hold, and the influence on degree of polymerization would be quite different.

In summary:

1. Given the existing mechanism, increasing H_2/CO ratio through the reactor has influenced the competition between polymerization rates and termination rates in such a way as to result in a decreasing degree of polymerization with reactor length.

2. Resolution of some of the assumptions incorporated into the existing mechanism may influence this result.

4.3.5 Reactor Comparisons

Since a model was not developed for the ebullating bed system, comparisons were limited to the tube-wall, slurry, and entrained bed reactors. The three areas concentrated on were as follows:

1. The base operating conditions chosen for each reactor system.

2. At the base conditions, the efficiency of utilization of CO and H_2 as well as the quantities of H_2O, CO_2 and hydrocarbon produced.

3. The sensitivity of CO conversion and degree of polymerization to operating condition changes.

The first of these comparisons is presented in Table 4.3-18. The slurry operating conditions and yields represent those given by Koelbel for a demonstration unit of 10,000 liter capacity (20). The entrained bed operating conditions and yields are taken from the Standard Oil of Indiana Feasibility Study performed by Kellogg (4). The tube-wall conditions were originally going to be taken from the Ralph M. Parsons study (16); however, as mentioned in Section 4.3.2, these conditions appeared to be overly optimistic. Two sets of conditions are shown for the tube-wall and are those that bracket the final operating conditions selected for the engineering evaluation. For each reactor type, the final selection appears to represent the most optimistic set of operating conditions, assuming present day catalysts.

There are three representations of reactor efficiency in Table 4.3-18, i.e., J factor, gas hourly space velocity, and β. Respectively, they represent the utilization efficiencies of catalyst surface, reactor space, and catalyst weight.

A comparison of GHSV's suggests that the entrained bed reactor utilizes reactor space roughly 3-1/2 times more efficiently than either the slurry or tube-wall reactor. The reason is the higher catalyst density per unit volume in the entrained bed reactor. However, this can be misleading, since the entrained bed reactor has an additional vessel which acts solely as a temporary holding tank for circulating catalyst. If one were to recalculate the GHSV using the volume of reactor plus holding tank, the value would decrease to roughly 350 hr^{-1}, and would not look nearly as attractive.

From a catalyst perspective, a comparison of β's suggest that the slurry and entrained bed reactors utilize a pound of catalyst roughly 4-1/2 and 2-1/2 times, respectively, as efficiently as the tube-wall reactor. At the same time, the J factor indicates that the catalyst

surface available for that pound of catalyst is roughly between 5 and 8 times as great for the slurry and entrained bed as for the tube-wall system.

It is apparent that the tube-wall reactor design is least efficient with regard to both reactor space and catalyst utilization. Regarding the remaining two systems, the entrained bed system seems to have a slight edge in the utilization of reactor space while the slurry system is clearly the most catalyst efficient.

One of the most important questions asked during the evaluation of these reactor systems was -- How efficiently does each reactor system convert CO and H_2 to usable product? To answer this question, a comparison was made at "base case" conditions for each reactor system. In the case of the entrained bed and slurry reactors, the base case was the Kellogg (4) and Koelbel (7) designs, respectively. In the case of the tube-wall reactor, the base case consisted of feed and product yields from the Parsons design (16) modified to represent potassium-promoted taconite as catalyst.

Table 4.3-19 represents reactant conversion and product yields per mole of fresh feed and per mole of CO plus H_2 converted. A comparison of total weight of hydrocarbon produced per mole of fresh feed suggests that the entrained bed reactor makes more product than the slurry reactor, which makes more product than the tube-wall reactor. Although these numbers may represent the performance of each specific reactor, they do not reflect the performance of the overall reactor systems for conversion of synthesis gas. For example, the entrained bed reactor uses a large amount of recycle gas and conversion is therefore higher on a fresh feed basis than for the other two reactors. The tube-wall reactor has a high feed gas H_2/CO ratio and this results in a lower synthesis gas conversion than in the slurry reactor. Variations in feed compositions also affect the figures in Table 4.3-19.

If moles of CO plus H_2 converted is used as a basis, the influences of feed compositions and water-gas shift can be eliminated. For every

mole of CO converted via water-gas shift, for example, a mole of H_2 is produced and, therefore, the sum of H_2 plus CO remains unchanged. A comparison of total weight of hydrocarbon produced on this basis shows only minor differences between reactor systems. However, the efficiency with which the shift reaction is being used is clearly shown by the relative consumptions or productions of H_2, CO, H_2O, and CO_2.

In the case of the entrained bed system, the CO_2 level in the combined feed, caused by high concentrations in the recycle gas, is so high that the shift reaction is at equilibrium, i.e., no CO_2 produced. Virtually every mole of CO entering the reactor is converted to hydrocarbon product. On the other hand, not one mole of H_2 is being produced within the reactor. The net result is that a large water-gas shift system is required upstream of the entrained bed reactor in order to supply the necessary hydrogen for feed.

In contrast, the shift reaction in the slurry reactor is far from equilibrium as reflected by the CO_2 produced. A significant portion of the CO is being converted to CO_2 in order to produce the necessary hydrogen, but the weight of hydrocarbon produced is equivalent or perhaps slightly greater than the other systems. Also the shift reaction is taking place in the same vessel as the Fischer-Tropsch reaction. Auxiliary equipment for adjustment of H_2/CO ratio is, therefore, not necessary, and as steam for the shift system does not have to be produced, an overall advantage in thermal efficiency will result.

The tube-wall reactor falls in between. This reactor requires a high H_2/CO ratio in the feed and, therefore, requires auxiliary shift reaction equipment. At the same time, the CO_2 content of the feed is not high enough to prevent the production of unneeded H_2 at the expense of CO. The combination of these two effects causes the tube-wall system to produce significantly less hydrocarbon per mole of fresh feed than the other systems.

The third set of comparisons, i.e., sensitivity of CO conversion and degree of polymerization to operating conditions, is represented in

Figures 4.3-35 through 4.3-41. The study was performed by adjusting either pressure, temperature, or H_2/CO ratio while maintaining all other base conditions constant.

Pressure can be seen to have a dramatic effect on CO conversion for both the entrained bed and tube-wall systems. The slurry system, however, is only modestly influenced. The insensitivity of the slurry system is caused by: a) back-mixing of the liquid phase which causes the concentration driving force for reaction to be constant and equal to the outlet conditions, and b) solubilities in the liquid phase. At 300 psig, the CO conversion in the slurry system is 94.5%. The liquid phase CO and H_2 concentrations are 6.5×10^{-4} and 8.5×10^{-4} moles/ft^3 liquid, respectively. At 174 psig, the conversion is 85% and the CO and H_2 concentrations are 8.4×10^{-4} and 5.23×10^{-4}, respectively. The rate of conversion is proportional to the product of these concentrations. At 300 psig this is 5.52×10^{-7}, while at 174 psig this is 4.39×10^{-7}. The ratio of these numbers is 1.26 and is a measure of the relative increase in driving force for CO conversion due to increased pressure. In the gas phase, this same ratio would be equal to the ratio of the pressures or 1.67. Clearly the liquid phase response to pressure is less dramatic than for the gas phase.

The decrease in the degree of polymerization with pressure in the slurry system (Figure 4.3-36) can be explained in a similar manner. As mentioned earlier, the degree of polymerization is determined by competition between rates of termination and polymerization. The rate of polymerization is generally described as being proportional to the product of H_2 and CO concentrations, i.e., $r_p \propto [CO]\,[H_2]$, while the rate of termination is proportional to just the H_2 concentration, i.e., $r_t \propto [H_2]$. For a gas phase system, when the pressure is increased from 174 psig to 300 psig, these concentrations at the reactor inlet increase in direct proportion to the absolute pressure by a factor of 1.67. The competition between polymerization and termination is, therefore, changed by a factor of 1.67 consistent with the ratio of r_p to r_t. In the slurry system, the solubility changes with respect to pressure coupled with the relative conversion levels determine the liquid phase concentrations and, therefore, the

relative rates. Solubility alone is roughly proportional to pressure, and one would, therefore, expect to see an increase in concentrations similar to the gas phase systems. However, the increased pressure also increases conversion thereby lowering the outlet concentrations. From 174 to 300 psig, the net result is a decrease in CO concentration from 8.4×10^{-4} to 6.5×10^{-4} moles/ft^3 liquid and an increase in H_2 concentration from 5.23×10^{-4} to 8.5×10^{-4} moles/ft^3 liquid. This corresponds to factors of 0.77 and 1.63 for changes in the CO and H_2 concentrations, respectively. The ratio of r_p to r_t, i.e. 0.77 x 1.63/1.63 = 0.77, reflects an increase in the role of termination relative to polymerization and is consistent with a decreasing degree of polymerization.

The influence of temperature on CO conversion and degree of polymerization is presented in Figures 4.3-37 and 4.3-38. As in the case of pressure, CO conversion in the slurry reactor is less sensitive to temperature than in the other two systems. The back-mixed nature of the slurry system results in reaction rates being dependent on outlet concentrations of reactants. Because these concentrations are low, the rates are much slower than in the other systems. Conversion is attained by using longer residence time, rather than by having the higher concentration driving forces of the plug flow reactors. This lethargic nature of the slurry reaction rates is reflected in the response of CO conversion to temperature.

There are few operating variables that have a more dramatic effect on degree of polymerization than temperature (Figure 4.3-38). The reason lies in understanding the competition between rates of polymerization and hydrogenation as they relate to the rate constants. The rates of polymerization and hydrogenation are proportional to Arrhenius rate constants with activation energies of 26,430 and 28,825 Btu/lb mole, respectively. An increase in temperature from 500°F to 600°F increases the polymerization and hydrogenation rate constants by factors of 3.71 and 4.17, respectively. Thus, the ratio of polymerization to rate of termination decreases to 0.89 of its original value, which causes the degree of polymerization to decrease with increasing temperature.

Although the above discussion satisfactorily explains the direction of change, it does not explain the insensitivity of the entrained bed reactor system relative to the slurry or tube-wall systems. The slurry reactor was defined as being isothermal. Although the tube-wall reactor was not defined in this manner, the heat transfer coefficient for heat removal was such that nearly isothermal conditions were attained. The entrained bed system was the only system which had three areas of increasing temperature through the reactor. But why would this cause the entrained bed yield structure to be less sensitive to temperature? Figure 4.3-42 illustrates the reason. Line I represents the degree of polymerization versus temperature line which would exist under isothermal conditions. Earlier it was mentioned that increasing the temperature from 500 to 600°F increases the termination rate constant by a factor of 4.17. When the same ΔT is applied from 600 to 700°F, the termination rate constant only increases by a factor of 3.28. In other words, the influence of increasing temperature at low temperatures is greater than at high temperatures. The entrained bed system was operated with a constant 36°F ΔT across the reactor at each inlet temperature. At T_1 on Figure 4.3-42, this 36°F ΔT will have the effect of dropping the degree of polymerization from point a to point b. At T_2, the same 36°F will have less effect and will only drop the degree of polymerization from point c to point d. The same applies for T_3. The net result is Line II which has a slope much less steep than the isothermal line.

The influence of combined feed H_2/CO ratios on CO conversion and degree of polymerization is presented in Figures 4.3-39 and 4.3-41. Not surprisingly, an increase in H_2/CO ratio results in an increase in CO conversion. Both the rates of polymerization and termination are proportional to H_2 concentration, and although the concentration of CO does drop with increasing H_2/CO ratio, its influence is surpassed by that of increasing H_2 concentration. It is interesting, however, that the increase in CO conversion between 1.0 and 2.0 H_2/CO ratios is significantly less than between 0.7 and 1.0 H_2/CO ratios, particularly in the tube-wall and slurry reactors. A closer look at the water-gas shift reaction explains this phenomenon. The CO conversion in Figure 4.3-39 is a combination of that converted to hydrocarbon and to CO_2 via the shift reaction. As the H_2/CO

ratio is increased, the reaction of CO and H_2O to form H_2 and CO_2 is inhibited. Obviously, this influence is greater from 1.0 to 2.0 H_2/CO ratio than from 0.7 to 1.0 H_2/CO ratio. In Figure 4.3-40 the shift reaction has been normalized out of the results, and only CO conversion to hydrocarbons is reported. It can be seen that, now, the influence of H_2/CO ratio is equivalent for the entrained bed and tube-wall reactors. The slurry reactor, however, is less sensitive. Here, as in the case of temperature, the back-mixed nature of the slurry system has resulted in slower rates causing less severe response to operating changes.

Although slurry back-mixing is responsible for slower rates, it is also responsible for the large influence of combined feed H_2/CO ratio on degree of polymerization. While in large part the plug flow reactor products distribution are being determined by near inlet H_2/CO ratios, i.e., 0.7, 1.0, and 2.0, the back-mixed reactor product distribution is being determined by outlet H_2/CO ratios, i.e., 1.15, 2.33, and 6.17. Figure 4.3-41 clearly reflects these results.